

## Marine CSEM of the Scarborough gas field, Part 2: 2D inversion

David Myer<sup>1</sup>, Kerry Key<sup>2</sup>, and Steven Constable<sup>2</sup>

### ABSTRACT

We explored the application of 2D inversion of marine controlled-source electromagnetic and marine magnetotelluric data to image an ambiguous target. The Scarborough gas reservoir off the west coast of Australia lies in close repose to a layer in the overburden of similar resistivity-thickness product and also is not far above the resistive basement, making it a difficult electric target. We found that the standard 2D smooth-inversion method yielded models that were unable to resolve this ambiguous structural configuration. We solved this problem by developing a two-step workflow, in which we first invert for a coarse background resistivity model (e.g., anisotropic layers), then invert for the minimum deviation from this background using a much finer model discretization. The main purpose of our two-stage workflow is to inject the knowledge into the inversion that the subsurface is composed of self-similar geologic domains. Though the resulting models did not resolve fine-scale structural details, they might still be used to map the overall extent and bulk qualities of a target in an otherwise confounding setting.

### INTRODUCTION

In a companion paper, Myer et al. (2012), we describe a marine magnetotelluric (MT) and controlled-source electromagnetic (CSEM) survey over the Scarborough gas field, on the northwest shelf of Australia (Figure 1). Myer et al. (2012) describe the CSEM data acquisition, processing, and quality, with particular attention to the data uncertainties derived from the data processing and analysis of the position and orientation uncertainties. An additional paper (Myer et al., 2013) describes the inversion and interpretation of

the MT data; although MT data are used in all the inversions presented here, a discussion of the deeper crustal structure derived from the MT data is omitted because our new results agree with this previous work. In this paper, we examine the CSEM data set in more detail and carry out interpretation using 2D regularized inversion with the specific aim of characterizing the shallow structure (approximately 3 km), in which the gas reservoir resides.

The Scarborough gas reservoir is located near the middle of the Exmouth plateau where the local geology is composed of primarily horizontal sedimentary layers of large extent. The average depth of the seabed is 950 m with approximately 50 m of bathymetric relief over the survey area. The reservoir consists of stacked sands located approximately 1 km below the seafloor. Figure 2 shows a simplified diagram of the expected resistivity structure of Scarborough. Of particular concern to CSEM exploration is the presence of a confounding resistive layer (the Gearle siltstone) approximately 200–300 m above the reservoir. Seismic surfaces show the Gearle to be a nearly constant ~100 m thick in the Scarborough area, and the five exploratory wells yield a resistivity of 3  $\Omega\text{m}$ . The resistivity thickness product of the reservoir ( $T_{\text{Gas}}$ ) is expected to be approximately 900  $\Omega\text{m}^2$ . This is not much larger than that of the confounding layer in the overburden ( $T_{\text{Gearle}} \sim 300 \Omega\text{m}^2$ ). Although the CSEM method is based on the physics of electromagnetic (EM) induction (Chave and Cox, 1982; Ward and Hohmann, 1987; Loseth et al., 2006; Andreis and MacGregor, 2008), the sensitivity to a resistive layer is dominated by a strong galvanic response (e.g., Weidelt, 2007) rather than inductive attenuation, hence CSEM data are generally more sensitive to the product of resistivity and layer thickness than to either parameter alone (e.g., Constable and Weiss, 2006; Key, 2012). Having a layer of similar  $T$  in close proximity to the target layer raises the possibility that the CSEM method may not be able to resolve the target very well.

This paper is divided into the following sections. First, we investigate the expected biases and ambiguities of the Scarborough reservoir configuration using 2D inversion of a series of synthetic

Manuscript received by the Editor 19 September 2014; revised manuscript received 10 December 2014; published online 9 April 2015.

<sup>1</sup>BlueGreen Geophysics, Encinitas, California, USA. E-mail: dmyer@bluegreengeophysics.com.

<sup>2</sup>Scripps Institution of Oceanography, University California San Diego, La Jolla, California, USA. E-mail: kkey@ucsd.edu; sconstable@ucsd.edu.

© 2015 Society of Exploration Geophysicists. All rights reserved.

models. Next, we present a standard 2D inversion of several of the survey tow lines and discuss the obvious artifacts and low resolution in view of the synthetic model results. Finally, we present a method to overcome these difficulties to arrive at a reasonable result when the target layer is confounded or of small  $T$ . Throughout this paper, we use the freely available parallel 2.5D adaptive finite-element inversion code MARE2DEM (Key and Oval, 2011), which relies on a new implementation of the Occam method of regularized inversion (Constable et al., 1987). The regularization used, except where otherwise specified, is the L2-norm.

## SYNTHETIC TESTS

We evaluated several synthetic studies to characterize the resolution we should expect to see from the inversions of real data and to constrain the biases and ambiguities introduced by our particular survey layout. All of the synthetic data sets evaluated in this section were created for the frequency coverage (0.25, 0.75, 1.75, and 3.25 Hz) and geometric configuration actually used in the survey (e.g., instrument position, source geometry, and data coverage). Further, these synthetic data sets use the error structure derived for the real data as defined in detail in the Myer et al. (2012) study and recapped in the section “Data inversion.” Gaussian noise is added to

the synthetic data sets, such that sigma of the random distribution is scaled by the data uncertainty for each datum.

## Layered versus monolithic water

The conductivity of ocean water varies with depth, typically decreasing rapidly in shallow water then stabilizing below the thermocline. Scarborough water depth averages 950 m, which is well below the thermocline on the Exmouth plateau. Including a finely layered ocean conductivity profile in a model increases the computational burden because these additional layers are discretized with a significant number of finite elements. Hence, we tested whether it is necessary to use a detailed water conductivity structure, or if just using the conductivity near the seafloor for the entire water column is sufficient.

For this survey, we use the Scripps undersea electromagnetic source instrument (SUESI) deep-tow vehicle, which records continuous measurements of seawater properties. SUESI was raised and lowered through the water column between each of the 18 tows, yielding a rich data set of measurements of the water conductivity from surface waters down to a towing depth of approximately 50 m above the seafloor. We found the depth-conductivity profile to be stable over time throughout the survey and produced the profile shown in Figure 3a. We constructed two models using the seafloor resistivity structure shown in Figure 2 and the actual transmitter and receiver positions for line 2 (see Figure 1). One model used only the bottom water conductivity, the other used layered conductivities. We calculated the normalized difference in the response of the two models:  $\sum(r_{1i} - r_{2i})/\sigma_i$ , where  $\sigma_i$  is the uncertainty for the  $i$ th datum,  $r_{1i}$  is the amplitude or phase response of the  $i$ th datum for model 1, and similarly for  $r_{2i}$ . Figure 3b shows the results for all ranges as a function of frequency, and Figure 3c shows results for all frequencies as a function of the source-receiver range. These indicate that using a simple water model introduces a bias in phase. Although this bias is within the error bars on a frequency-by-frequency basis, it is significantly larger than the error bars for middle ranges, indicating that accurate representation of the entire ocean conductivity profile is important even for moderately deep water depths of order 1 km.

## Isotropic versus anisotropic inversion

In an area composed of stacks of thin layers of varying resistivity, the bulk electric conductivity sensed by CSEM data can appear anisotropic. Because the transmitted EM field forms large vertical loops about the source dipole, even inline data collected on 2D profiles are sensitive to this type of layered anisotropy (e.g., Constable, 2010; Ramananjaona et al., 2011; Brown et al., 2012; Ray and Key, 2012). However, adding anisotropy to inversion increases the number of parameters and nonuniqueness in the inverted structure because anisotropic features can often trade off

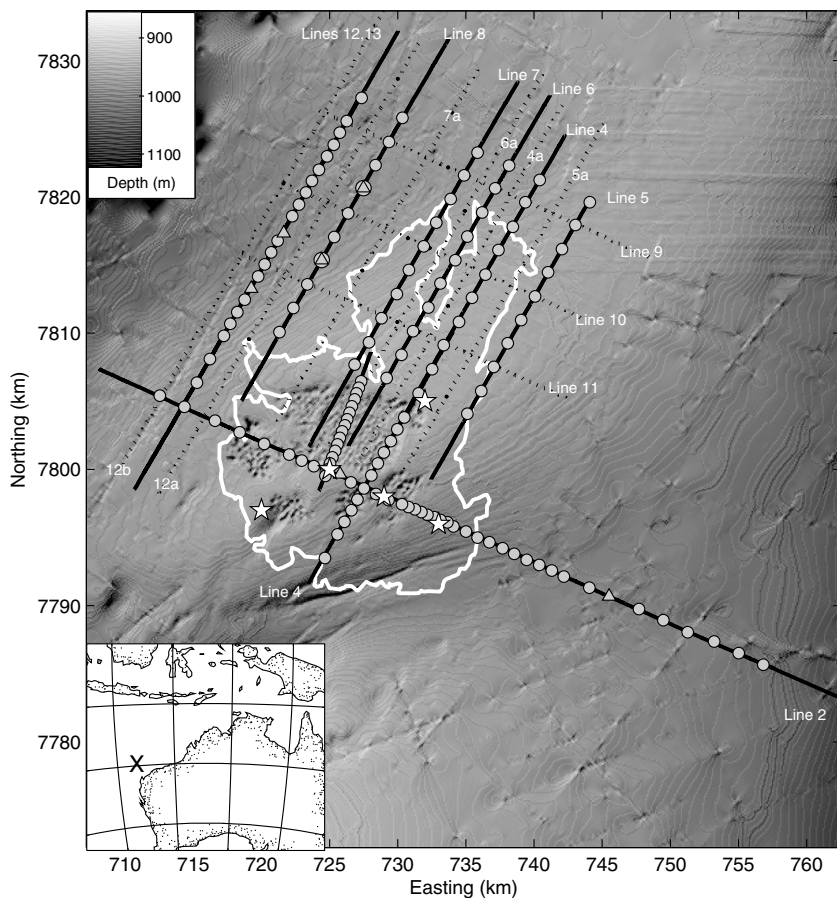


Figure 1. A bathymetric map overlain with the Scarborough instrument deployment locations (filled circles), predicted reservoir outline (white), exploration wells (stars), and tow lines (black lines). The inset shows the survey location off the west coast of Australia. The primary tow lines are solid lines, and the secondary tow lines are dotted.

with isotropic layering; typically, anisotropic inversions appear much smoother than their isotropic counterparts for a given structure. Thus, it is possible that an anisotropic inversion might interpret isotropic layering as anisotropy and consequently not resolve thinly layered structures. To test the efficacy of anisotropic inversion in the Scarborough geology, we constructed two models based on tow line 2 and the resistivity model in Figure 2; one model is isotropic, and the other is anisotropic with the vertical resistivity set to 1.5 times the horizontal resistivity. Synthetic data generated from each model were then inverted for isotropic and anisotropic resistivity, in which the anisotropy was parameterized using transverse isotropy in the vertical direction (TIZ, where  $\rho_x = \rho_y \neq \rho_z$ ). This yielded four inversions in all. Note that although the synthetic data were generated from layered models, the inversions were performed with a model space discretized laterally and vertically.

Figure 4a shows representative vertical profiles taken from the isotropic forward model and the isotropic and TIZ anisotropic inversions of the isotropic synthetic data. Both inversions perform equally well. Note that the TIZ inversion derived essentially no anisotropy, indicating that for this configuration, at least, there is no confusion between layering and anisotropy.

Figure 4 shows vertical profiles for the horizontal (Figure 4b) and vertical (Figure 4c) resistivity of the anisotropic forward model and the two inversions. Note that the isotropic inversion of the anisotropic model oscillates between fitting the horizontal resistivity in some depth ranges and the vertical in others. It also includes some spurious structure in the shallowest section as it attempts to compensate for the anisotropy. The TIZ inversion, on the other hand, fits both modes of resistivity well and does not develop any spurious structure or abnormal anisotropy.

These results indicate both that the inline-only CSEM data carry information about anisotropy and that a TIZ inversion can adequately resolve it without introducing invalid structures when the data are isotropic.

### Site spacing

Part of the experimental design for the Scarborough survey was a test of site spacing with respect to the burial depth of the target. For most of the sites in the northern area, the site spacing is 2 km or wider, which is generally thought to be too wide for a target that is less than 1 km below the seafloor. However, there is a high density of 3D information in this area (i.e., non-inline tows and crossing lines) and we expect to address the trade-off between 3D inversion and site spacing in a future publication. For the purposes of the present work, we address the effect of site spacing on 2D inversion using the configuration of line 2, in which site spacing varies from 500 m to 4 km.

We created an anisotropic model ( $\rho_z = 1.5\rho_{x,y}$ ) of line 2 including the gas reservoir (Figure 5a) and calculated synthetic data with the same distribution as the real data, then inverted it with a TIZ inversion (Figure 5b). Whenever the site spacing exceeds the depth of the target (approximately 1 km), the horizontal layering breaks into segments giving the appearance of vertical stripes in the model. To rule out mesh artifacts, the model blocks have a uniform size (250 m wide and 100 m tall) down to a 5-km depth. We attempted to minimize the segmenting by biasing the roughness penalty against horizontal variations. In Figure 5b, we show the result when there is a 3:1 penalty against horizontal versus vertical model roughness. We varied this penalty bias up to 10:1 with little appreciable

difference in the resulting model. Clearly, the site spacing poses a significant problem for interpreting the Scarborough inversion results, especially in view of the fact that almost all lines use site spacing that is twice the target depth.

### Confounding overburden layer

The expected geologic configuration at Scarborough contains an anomalously resistive layer in the overburden (the Gearle siltstone) approximately 300 m above the target gas reservoir. Well logs show the Gearle layer to contain no hydrocarbons, so in terms of CSEM exploration, its presence across the prospect presents a potential hindrance to interpretation. Because the resistivity thickness product of the Gearle is similar to that of the thickest part of the reservoir ( $T_{\text{Gearle}} \sim 300 \Omega\text{m}^2$  and  $T_{\text{Gas}} \sim 900 \Omega\text{m}^2$ ) and they lie in close proximity, it is possible that inversion of the CSEM data will be unable to distinguish between the two separate layers. The 2D site-spacing test (Figure 5) gives an indication of that, although it is uncertain whether or not that particular test's inability to separate the layers is due primarily to site-spacing and data distribution effects.

We created a series of 1D synthetic tests to determine whether with a perfect configuration, the confounding and target layers can be resolved separately and, if so, at what separation distance that occurs. For each test, we started with a 1  $\Omega\text{m}$  half-space containing a confounding layer with  $T = 300 \Omega\text{m}^2$  at 700 m below the seafloor (the depth of the Gearle). We also added a target layer with

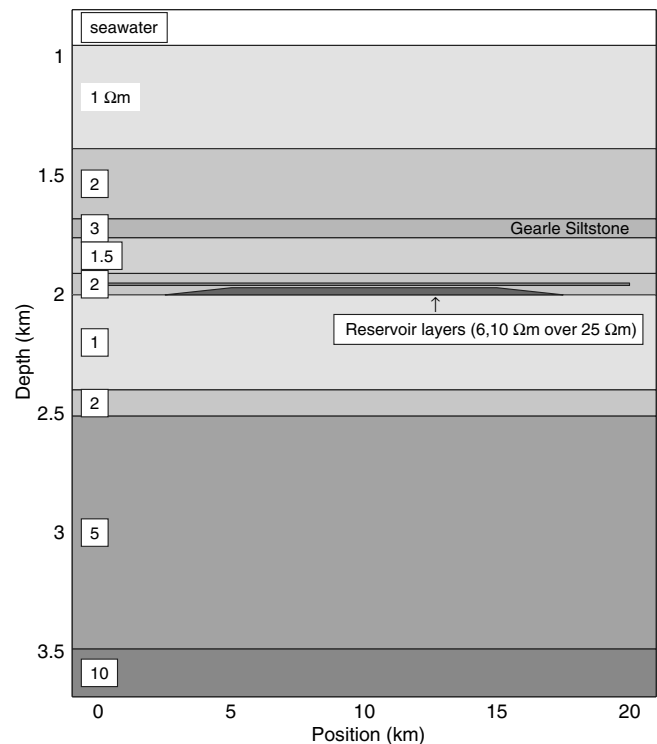


Figure 2. A simplified diagram of the expected geologic structure showing resistivities for each layer. The gas reservoir is not a monolithic body, but a stack of thin traps ranging from 6 to 10  $\Omega\text{m}$  overlying a larger approximately 25  $\Omega\text{m}$  body of varying thickness. The resistivity thickness product of the reservoir ( $T_{\text{Gas}}$ ) is expected to be approximately 900  $\Omega\text{m}^2$ , which is not very large compared with the overlying Gearle siltstone  $T_{\text{Gearle}} = 300 \Omega\text{m}^2$ .

$T = 900 \Omega\text{m}^2$  at a variety of separation distances below the confounding layer ( $\Delta Z = 300$  to  $700$  m). Each synthetic data set was then inverted using a freely available 1D CSEM implementation of the Occam method (Key, 2009).

Figure 6 shows the models resulting from five separate inversions. At a separation distance of  $\Delta Z = 300$  m, the inversion resolves only a single layer. By  $Z = 500$  m, a second layer has developed enough that an interpreter might reasonably consider it a layer and not an inversion artifact. But note that the depths of both layers are misplaced, indicating that the signals from the two separate layers are still being confused by the inversion. It is not until  $\Delta Z = 700$  m that the two layers move appreciably toward their correct depths.

It is intriguing to note that the 700-m separation distance at which the 1D inversion does well is also the burial depth of the confounding layer, suggesting that a rule of thumb regarding layer resolution and separation distance might be developed. However, we must caution against this. We ran several other suites of inversions to investigate the model space and found that although increasing the contrast between  $T_{\text{confound}}$  and  $T_{\text{target}}$  does not change the depth at which the two layers are separately resolved, increasing the actual value of  $T$  does. If  $T_{\text{confound}} = 1000 \Omega\text{m}^2$ , for example, then the two layers can be resolved when  $\Delta Z$  is approximately 300 m. Also, as the top depth of the confounding layer increases, the value of  $T$  must also increase to keep pace with the declining depth resolution

of CSEM. So, for example, a configuration with  $T_{\text{confound}} = 300 \Omega\text{m}^2$  at  $Z = 1000$  m is too deep for such a small  $T$  to be resolved even though this is just 300 m deeper than our original test case. Thus, the agreement between the 700-m depth and 700-m  $\Delta Z$  is purely coincidental. It appears that no rule of thumb can be derived here.

## DATA INVERSION

We separately inverted the data from seven different inline tows (lines 2, 3 + 4, 5–8, and 13). Each inversion uses a configuration informed by our synthetic tests: layered ocean conductivity structure, TIZ anisotropy, and a 3:1 bias against horizontal versus vertical variation in the roughness penalty. We used a uniform model mesh from  $\pm 2$  km beyond the end sites and down to 4 km below the seafloor. These mesh blocks are quadrilateral with approximate measurements of 250 m wide  $\times$  100 m tall and are deformed to match the seafloor then progressively flatten down to a level surface at 4 km. Outside of the quadrilateral mesh area, we revert to triangular elements which grow with distance out to model boundaries placed far from the area of interest. We used quadrilateral blocks in the area of interest instead of the usual triangular finite-element mesh for two reasons: First, it reduces the number of parameters to be solved for by about half, which is an important memory consideration in an Occam-style inversion in which an  $N \times N$  matrix must

be inverted, where  $N$  is the number of model parameters. Second, the geologic structure at Scarborough is composed predominately of horizontal layers and is better matched by an assemblage of quadrilateral blocks than by the rough horizontal surfaces approximated with constrained Delaunay triangulations.

The CSEM data for each inversion used an uncertainty structure described in detail in Myer et al. (2012). In brief, this is the random error derived from data processing, subject to an error floor that is specific to each instrument channel and frequency, added in quadrature with the position/orientation error derived from perturbation analysis. The absolute minimum error is set to 2%. The CSEM data from four frequencies (0.25, 0.75, 1.75, and 3.25 Hz) were used, and those with a transmitter-receiver offset  $< 1$  km were excluded, as were data with a signal-to-noise ratio of  $< 3$ . Data were decimated to transmitter positions spaced about every 250 m along the tow track. MT data for each tow line were also included.

Each inversion converged to an rms misfit of 1.0. Figure 7 shows the vertical resistivity model ( $\rho_z$ ) resulting from three of the inversions: lines 2 and 3 + 4 (a and b) are across the center of the gas reservoir, line 13 (c) is several km off the target. The horizontal resistivity ( $\rho_{x,y}$ ; not shown) is generally lower than  $\rho_z$  down to 2.5 km, then it is the same below that depth. The ratio of  $\rho_z$  to  $\rho_{x,y}$  is between one and two in the anisotropic section.

As predicted by the synthetic modeling, the horizontal layering is heavily segmented due

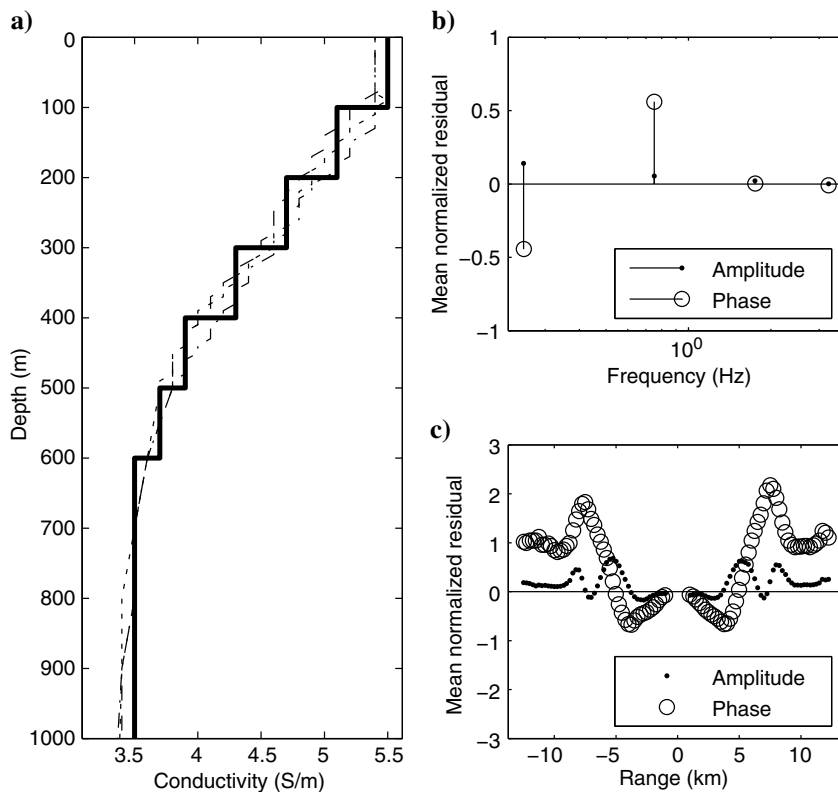


Figure 3. (a) The depth versus water conductivity profile for Scarborough. The solid line is the water conductivity model used in the inversions. The dotted lines are three examples from the beginning, middle, and end of the survey. (b) The normalized difference for all ranges by frequency and data type between a model with monolithic water conductivity and one with layered water conductivity. (c) The normalized difference for all frequencies by range and data type. Using a simple water model introduces a bias in phase, which is significant with respect to the data uncertainties.

to the site spacing. Also as expected, the Gearle layer is not separated from the gas reservoir in any of the inversions. Comparing Figure 7a with the synthetic inversion model of line 2 in Figure 5b, it is interesting to note that the basement resistivity shows up at a much shallower depth than expected. The expected resistivity structure on which the synthetic models are based is only informed by well logs down to the depth of the gas reservoir (2 km). Below that, resistivities are derived from seismic properties. Our CSEM + MT inversions consistently find the basement to be more resistive than expected. Although this might seem like a minor point, it is important in the case of Scarborough because it means that the reservoir “signal” is not only confounded by an overlying resistive layer, but it might also be confounded by close proximity to the resistive basement. We have, in effect, three resistive bodies in close repose: the Gearle approximately 300 m above the reservoir, which may be only approximately 500 m above the resistive basement.

## 2D INVERSION FOR AN AMBIGUOUS STRUCTURE

It is clear from the standard inversions that the ambiguity of the Scarborough configuration cannot be resolved with simple smooth inversion without any additional structural information added. There are many possible directions one can go in an attempt to solve this problem. The family of models that may fit the data equally well is infinite, so designing a workflow that can pick out inversion models that are more to the interpreter’s liking is always possible. However, we prefer the family of solutions that yield the least structure required to fit the data because this is tantamount to applying Occam’s razor. From such models, it is possible to draw conclusions about what is required at the very least and the interpreter has more solid ground on which to stand.

For Scarborough, the least-structure inversions show us merely that the level of ambiguity is great. They do not appear to be useful in constraining the extent of the reservoir or its lateral variations in quality.

Because these smooth models are not useful in this case, we consider a different class of models — those in which there is minimum deviation from a background resistivity structure. Suppose we have a priori knowledge of the resistivity of the strata in a survey area; for example, from a nearby well log. We can construct an inversion that is regularized not by overall smoothness but by least deviation from this a priori assumed background. This inversion would yield informa-

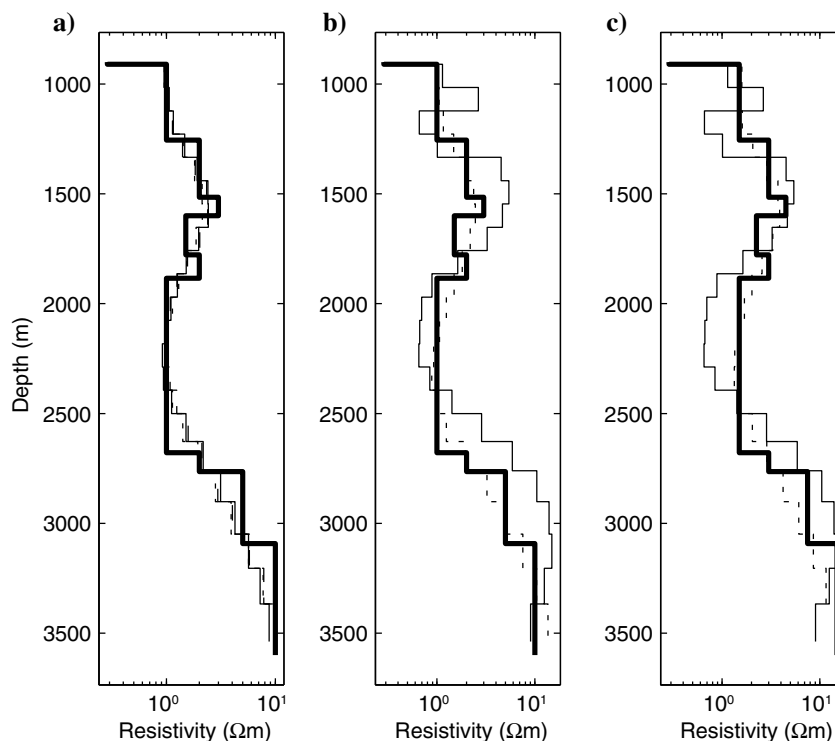


Figure 4. Representative vertical profiles taken from 2D inversion of (a) an isotropic model and (b) and (c) an anisotropic model. Panel (b) is the horizontal resistivity, and panel (c) is the vertical resistivity for the same anisotropic model. In each panel, the thick solid line is the true resistivity, the thin solid line is from the isotropic inversion, and the dotted line is from the anisotropic inversion. Note that panel (a) contains two dotted lines ( $\rho_{x,y}$  and  $\rho_z$ ), but they overlap because the anisotropic inversion did not confuse thin layers with anisotropy.

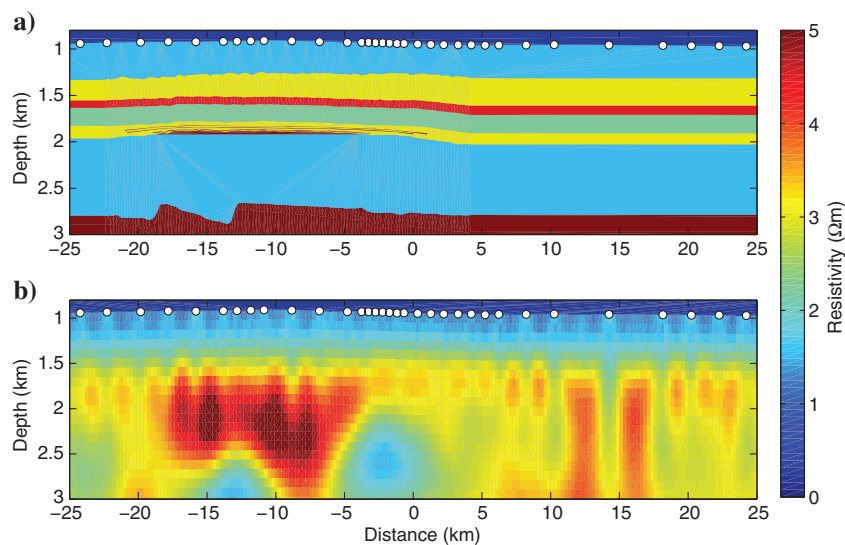


Figure 5. (a) Synthetic model of line 2 and (b) TIZ inversion. Site locations are indicated with open circles. The site spacing, which varies from 500 m to 4 km, introduces vertical stripes in the model everywhere except where the spacing is less than or equal to the depth of the target. In this particular inversion, the model blocks are 250 m wide  $\times$  100 m tall down to a 5-km depth, and there is a 3:1 bias against horizontal versus vertical variation in the roughness penalty.

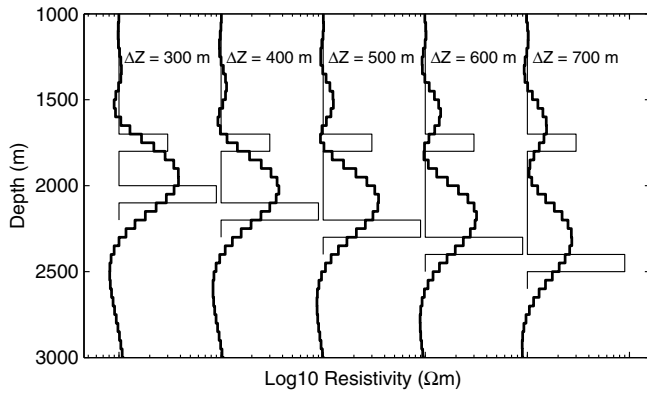
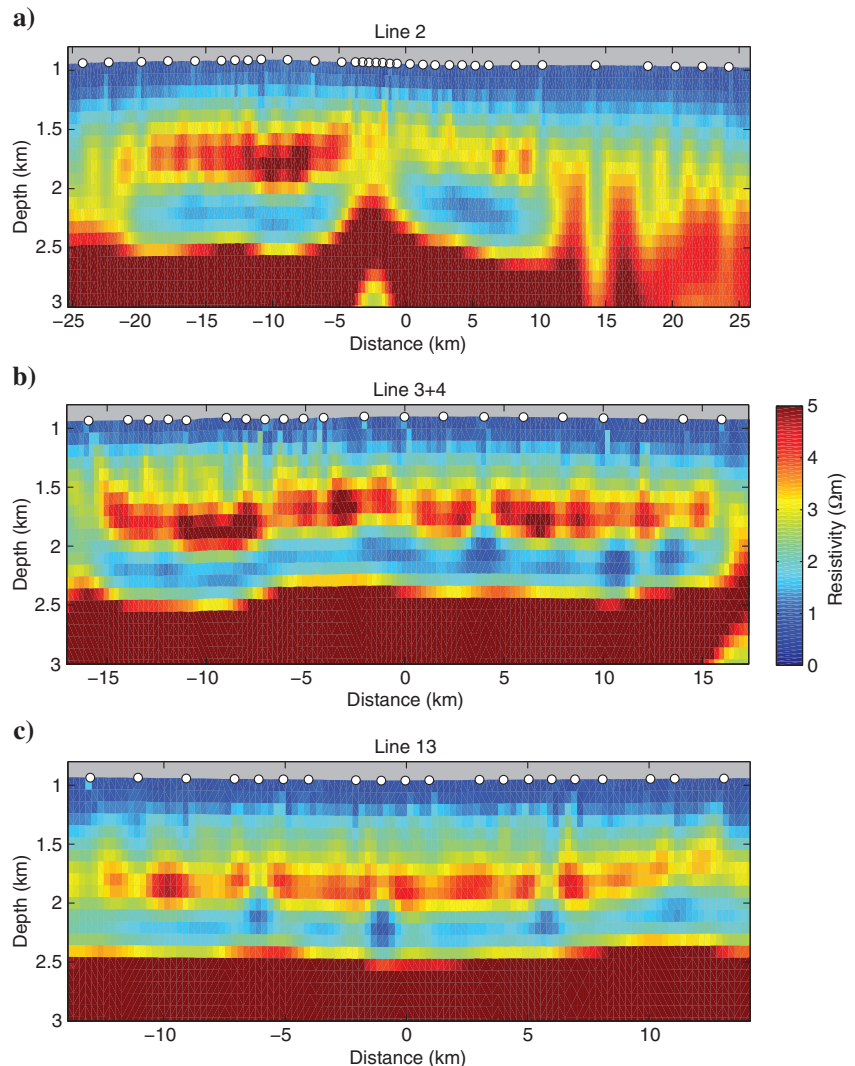


Figure 6. Five different 1D inversion tests of the resolvability of a target underlying a confounding layer given varying separation distances ( $\Delta Z$ ). The thin lines are the true models, and the thick lines the inversion model results. Each pair has been shifted along the  $x$ -axis by a decade for clarity. The transverse resistance for the target layer is set to three times that of the confounding layer in the overburden to mirror the expected configuration of the Scarborough reservoir.

Figure 7. Vertical resistivity models resulting from 2D inversions of (a) line 2, (b) lines 3 + 4, and (c) line 13. Open circles are the site locations. Horizontal resistivity (not shown) is generally lower down to 2.5 km. The models are mostly isotropic below that depth. Lines 2 and 3 + 4 run across the center of the reservoir. Line 13 is several km off the target.



tion about the unexpected or targeted bodies embedded in the subsurface (e.g., oil and gas).

However, we do not often have a priori knowledge of the background, and even in cases where we think we do, there is no guarantee that the values are correct (see the unexpected depth of the Scarborough basement in Figure 7). So, we have developed a workflow that inverts for ambiguous structure in two stages. First, we invert for anisotropic background resistivities with a highly sparse model mesh, and then we invert for deviation from this background with a more finely discretized model.

Using surfaces derived from a 3D seismic survey of the Scarborough prospect and deep layering determined from MT (Myer et al., 2013), we created a very sparse mesh of each tow line; i.e., there is only one model block for each geologic layer, 11 in all. Regularization of this mesh presents a problem in that we would like to allow for large jumps in resistivity from layer to layer by removing the roughness penalty. However, when the roughness penalty is removed, the remaining anisotropy penalty and broad resistivity bounds (0.01–10,000  $\Omega\text{m}$ ) are not enough to stabilize the inversion, which quickly develops alternating layers of conductors and resistors before failing. To regularize this inversion without

forcing smoothness across the layer resistivities, we narrowed the resistivity bounds on every layer to  $1 - 1000 \Omega\text{m}$  (except the conductive layer at a 10-km depth indicated by MT, whose bounds are 0.01–1000). The bounds and anisotropy penalties are weighted at one, whereas the roughness penalties are weighted at 0.1, so that they contribute in only a minor way to the overall regularization. We then run the inversion until it can no longer lower the rms misfit.

In the second stage of the workflow, we construct a more finely discretized model in which each layer is gridded with quadrilaterals whose horizontal surfaces deform gradually between the upper and lower seismic surfaces. These model blocks vary in thickness from approximately 80 m at the seafloor to approximately 1 km at a 9-km depth. We made the blocks approximately 1 km wide in an attempt to ameliorate the effects of our wide site spacing. Each model block was then assigned the anisotropic resistivities from the regional inversion as the starting values and prejudice values. The prejudice penalties are given weights of one. The resistivity bounds, anisotropy penalties, and roughness penalties are completely removed so that the inversion is only regularized by the prejudice. The functional being minimized is then simplified to  $U = \|m - m_*\|^2 + \mu^{-1} \left[ \left\| \frac{d-F(m)}{\sigma} \right\|^2 - \chi_*^2 \right]$ , where  $m$  is the inversion model resistivities,  $m_*$  is the prejudice model resistivities,  $\mu$  is the Lagrange multiplier, and the term in square brackets is the usual difference between the normalized data misfit and the target misfit.

We tested this workflow on data derived from the synthetic model shown in Figure 5a. Figure 8a and 8b shows the horizontal and vertical resistivities, respectively, from the first step in the workflow: TIZ inversion for the background. (Note that the color scale has been broadened compared with previous figures to prevent saturation in the figures from obscuring important details.) This inversion reached an rms misfit of 1.5. The horizontal resistivities are very similar to the true model, but with a slight elevation in the layer containing the reservoir and a misplacement of the Gearle resistivity (which should be just below 1.5 km) into its overlying layer. The vertical resistivities combine the Gearle and reservoir signal into the layer residing between them. Panels (c and d) show models resulting from the second step in the workflow: inversion regularized by a background prejudice only. Although this model consists of 2279 model blocks instead of just 11, the horizontal resistivity has not changed from the background. All the changes required to fit the data to rms 1.0 are in the vertical resistivity. The resistivity of the area between  $-5$  and 20 km distance and from the seafloor down to a 2.5-km depth has risen slightly to reflect the presence of the  $25 \Omega\text{m}$  layer of the reservoir. The less-resistive 6 and  $10 \Omega\text{m}$  extend further, laterally, and they are not reflected in the final inversion.

The portion of the resistive layer between 1.5 and 2 km depth and outside the bounds of the reservoir has become slightly more conductive

than the prejudice. This illustrates an interesting point about the differences in the two stages of the workflow. Because the sparse model is not discretized laterally, the resistivities derived for each layer are a function of the data coverage across the body of interest. As the percentage of data affected by the target increases, the layer resistivity will become more similar to the target resistivity. For line 2, we have roughly equal coverage on and off the reservoir, so the resistive layer gets an average resistivity for on and off the structure in the first stage of the workflow. Lateral differentiation occurs in the second stage. By breaking the workflow into two separate steps, we are adding into the inversion the knowledge that the earth is generally composed of a collection of self-similar geologic domains. Although these domains are layers in this example, they need not be. The first stage of the workflow can include any assemblage of sparse model blocks: intrusions, diapirs, steeply dipping layers, etc.

To illustrate the importance of the first stage of the workflow, we ran an additional inversion in which we regularized by a penalty

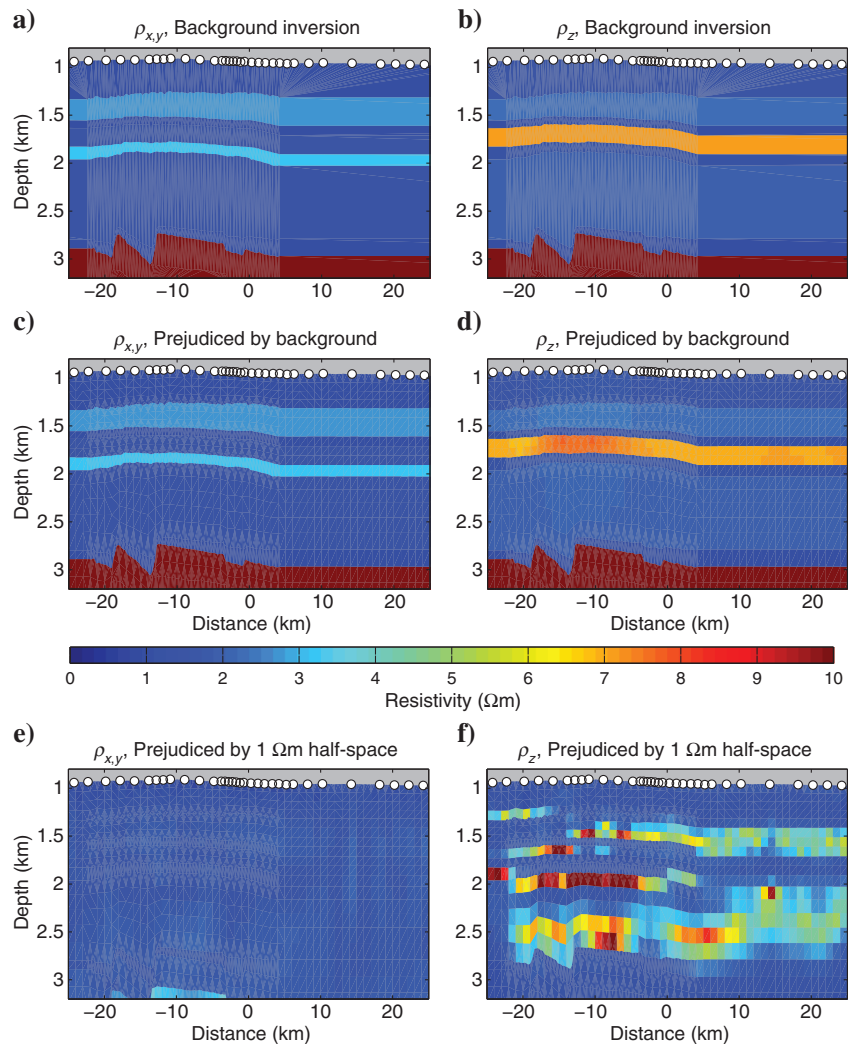


Figure 8. TIZ inversions of the synthetic data from the model in Figure 5a. (a and b) The horizontal and vertical resistivities of the extremely sparse (11 layers only) background inversion, (c and d) the discretized inversion regularized by a penalty against departure from the background inversion results shown in panels (a and b), and (e and f) the discretized inversion regularized by a penalty against departure from a  $1 \Omega\text{m}$  half-space.

against deviation from a  $1\text{-}\Omega\text{m}$  background. This is essentially a “minimum structure” model, in which instead of being constrained by smoothness, we want the least amount of resistivity required to fit the data. Figure 8e and 8f shows the models resulting from this one-stage inversion (converged at rms 1.0). The horizontal resistivity is featureless, having not derived any of the structure of the true model. The vertical resistivity is a series of blobby layers. Although there is elevated resistivity between 0 and  $-20$  km where the reservoir resides, there is no resolution of the basement or it is perhaps fragmented and misplaced at the 2.5-km depth.

We applied our new workflow to all seven 2D lines at Scarborough. Figure 9 shows the results for line 2. The first stage of the workflow reached rms 3.5 and yields the regional anisotropic resistivities shown in (a)  $\rho_{x,y}$  and (b)  $\rho_z$ . In terms of horizontal resistivity, the shallow structure is essentially conductive all the way down to the basement with most values below  $2\ \Omega\text{m}$ . This agrees with the geologic interpretation that these are horizontally oriented sands and siltstones. The vertical resistivities above the basement vary more widely yielding an approximately  $7\text{-}\Omega\text{m}$  layer between the

depths of the Gearle and reservoir and an approximately  $5\text{-}\Omega\text{m}$  layer down to the basement. Compared with the smooth inversion (Figure 7a), the basement depth has moved down to 3.0 km. This is an interesting change because it places the basement nearer to the 3.5-km depth of the original geologic model. Although this might indicate that our new workflow is sometimes better able to resolve features that are near the resolution limit of CSEM than a standard smooth inversion, it might also be coincidental — an artifact of choosing a different class of models in an ambiguous system.

Figure 10 shows depth profiles of the horizontal and vertical resistivities taken from the regional inversions of all seven lines. Note the general agreement between them all except at the ambiguous depths, where the Gearle and reservoir reside (1.5–2.0 km) and where the basement appears (2.6–3.2 km). We expect the Gearle/reservoir region to vary from inversion to inversion because of the variations in the reservoir and differing data coverage in each line. The basement variation from line to line is due to a 500-m shallowing of the basement-defining seismic layer toward the northern end of the survey area.

The prejudiced inversion for line 2 (Figure 9c) converges quite rapidly to rms 1.0. We only show the vertical resistivity model because, as in the synthetic study (Figure 8a and 8c), the horizontal resistivities are essentially unchanged from the regional inversion. Also as in the synthetic study, the model changes required to go from rms 3.5 to 1.0 are almost entirely in the “confounded layer” between the depths of the Gearle and reservoir. The resistivity of this layer decreases outside the reservoir bounds ( $\sim 4\text{--}5\ \Omega\text{m}$ ) and increases inside ( $\sim 10\ \Omega\text{m}$ ). The  $5\ \Omega\text{m}$  layer below it has also become slightly less conductive to the right ( $3.5\text{--}4\ \Omega\text{m}$ ) outside the suspected reservoir bounds.

This pattern of differences between the regional inversion and prejudiced inversion (minimal change in  $\rho_{x,y}$ ; changes in  $\rho_z$  primarily in the confounded region) is common to all seven inversion scenarios. Line 2 is the best case, however, because its changes are focused between 1.5 and 2.0 km depths. This is no doubt a consequence of the good data coverage and large lateral extent. The other lines experienced changes in the slightly broader depth range of 1.2–2.2 km and a few showed some variations in the basement.

Because most of the lines trending north-south have a 2-km site spacing, interpretation of their inversion models is hampered by the segmentation observed in the synthetic study. Instead, we integrate the resistivity of the top 1.2 km of seafloor (Figure 11). The horizontal resistivity-thickness product ( $T_{x,y}$ ) is more-or-less uniform across all inversions.  $T_z$ , however, exhibits variations up to approximately  $1000\text{--}1200\ \Omega\text{m}^2$  above the background, which is near the value expected for  $T_{\text{gas}}$  of  $900\ \Omega\text{m}^2$ . So, even though we are unable to distinguish the depths of the various resistive layers in each

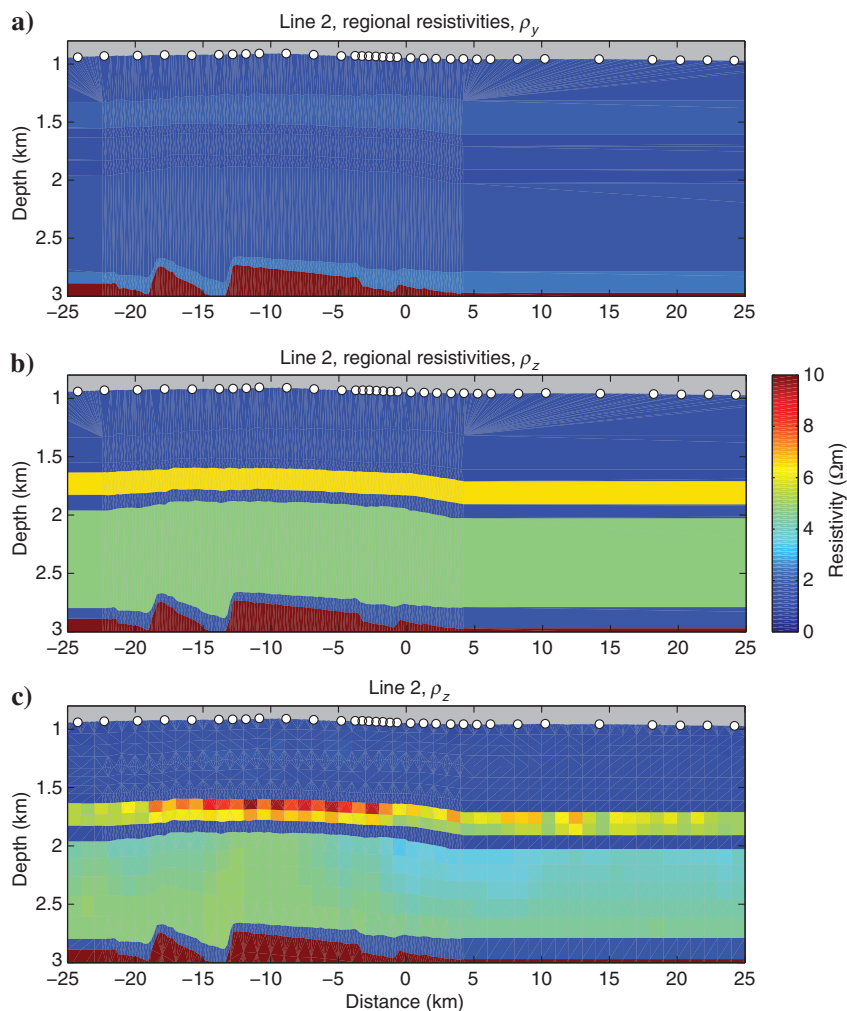


Figure 9. The models resulting from the regional and prejudiced inversions of line 2: (a) The horizontal resistivity and (b) vertical resistivity of the regional (11 layer) model, which fits the data to rms 3.5. (c) The vertical resistivity of the prejudiced inversion, which started from the regional inversion and converged to rms 1.0. There were negligible changes in the horizontal resistivity (not shown).

inversion, we can still derive a quantitative measure of the extent of the reservoir.

The outline shown in the figure is the expected gas-water-contact boundary as defined by a particular depth contour on a seismic sur-

face. Across the main body of the reservoir, the area of high  $T_z$  is a few kilometers smaller in the east indicating that the body of the reservoir is narrower than expected. The two “rabbit ears” in the north have been interpreted as channel sands, and one of the original survey goals was to determine if the gas extended into these channels.  $T_z$  from the 2D inversions shows gas extending into the eastern channel but only slightly into the western channel, indicating that perhaps the western channel has low concentration or is pockets of gas only. However, we also show resistivity extending on a broad scale east of the eastern channel. The easternmost north–south line has values of  $T_z$  similar to the line that runs straight up the center of the channel, so it is more likely that this is an extension of the gas beyond the predicted seismic depth contour and not a “broadside swipe” of the gas in the channel. If that is the case, then either the wrong seismic depth contour has been chosen or the seismic surface is incorrect in this area. Of course, it is also possible that the increase in  $T_z$  is due to a thickening of the Gearle siltstone layer, which would enhance the resistivity-thickness product without the need to interpret more gas. We expect that future work on the full 3D data set may give more details as to the extent of the gas in the vicinity of the rabbit ears.

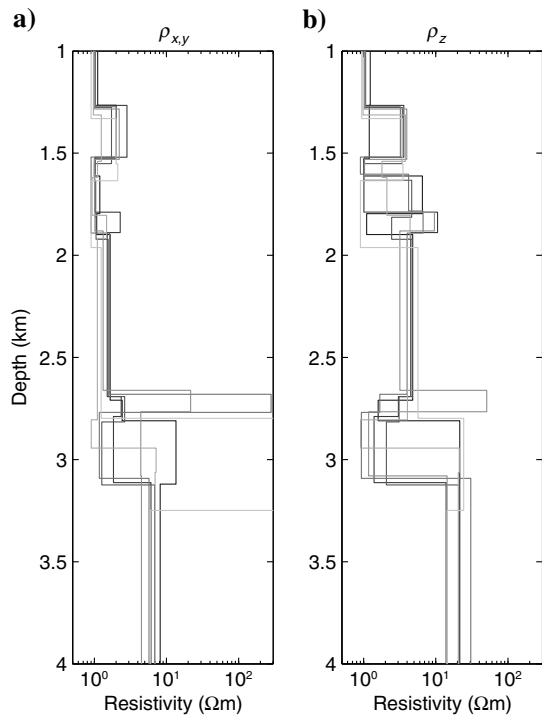


Figure 10. Vertical profiles of (a) horizontal and (b) vertical resistivity taken from the regional inversions of the seven Scarborough lines. The lines are unlabeled because their specific values are unimportant. Note the general agreement everywhere except in the ambiguous region, where the Gearle and reservoir reside (1.5–2.0 km) and where the basement appears (2.6–3.2 km).

CONCLUSIONS

Our 2D inversion of the Scarborough survey CSEM and MT data showed that because of the close proximity of several resistive layers, the standard smooth inversion is too ambiguous to resolve the gas reservoir from an overlying resistive layer and underlying resistive basement. Additionally, we have shown that the survey site spacing has an unfortunately deleterious effect on the competency of horizontal layers at the depths we are interested in.

We have developed an alternative workflow, which we suggest may be useful in cases where the necessary structural resolution is not expected to be obtained by CSEM. In the first stage of this workflow, one inverts only for the background resistivity of individual layers. In our work, we defined these layers by seismic surfaces, but in the absence of these, a geologically reasonable analog might also suffice. For the background inversion, the roughness penalty is scaled down to 0.1 and the inversion is primarily regularized by the anisotropy penalty and narrow bounds on resistivity. Anisotropic resistivities derived in the first stage are then used as the starting model and prejudices for the second stage inversion. Here, the inversion is regularized by the prejudices alone. This workflow results in a model that is minimally different from the background model as opposed to the standard inversion, which is maximally smooth. The main purpose of our two-stage workflow is to inject the knowledge into the inversion that the subsurface is composed of self-similar geologic domains.

Also, although this workflow is still subject to the resolution limits of CSEM (i.e., ambiguous structures are still ambiguous), there is a hint that it might do a better job at separating structures that are near the limits of resolution. The maxi-

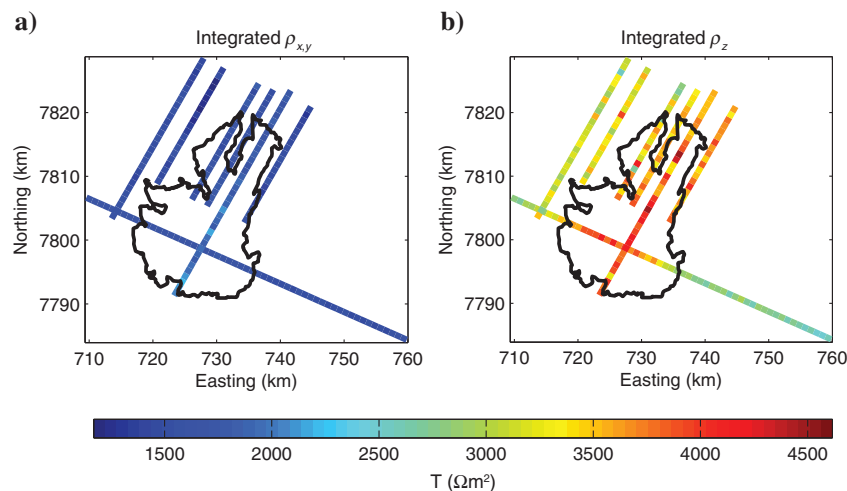


Figure 11. Integrated (a) horizontal and (b) vertical resistivity of the top 1.2 km from all seven 2D inversions. The outline is the expected gas-water contact taken from a seismic depth contour. The extent of the gas is not as broad in the main body of the reservoir as expected, and the western channel contains either lower concentrations or only pockets of gas. There is a high concentration of resistivity in the eastern channel, and this continues eastward out of the expected boundary.

mally smooth inversion blurs such structures in a trade-off between data fit and roughness.

We applied this workflow to Scarborough and showed that the CSEM data indicate that the reservoir extent is not exactly as expected from the gas-water contact outline derived from seismics. The higher concentrations of gas are constrained to a slightly smaller area in the main body of the reservoir, but there is more resistivity than expected around the easternmost of the two channel sands.

### ACKNOWLEDGMENTS

The authors are grateful to BHP Billiton Petroleum for funding the data collection and G. Liu and M. Glinsky of BHP for providing the background information we needed for the experimental design phase. We also thank the Scripps Seafloor Electromagnetic Methods Consortium for providing funding for the analysis and inversion phase of this project. The captain, crew, and scientific party of the *Roger Revelle* worked hard to make this project a success, and we thank them all. We also thank BHPB, Shell, Esso Australia, and Chevron for providing ingress permissions for this survey. We thank the editor and reviewers for their helpful comments.

### REFERENCES

- Andreis, D., and L. MacGregor, 2008, Controlled-source electromagnetic sounding in shallow water: Principles and applications: *Geophysics*, **73**, no. 1, F21–F32, doi: [10.1190/1.2815721](https://doi.org/10.1190/1.2815721).
- Brown, V., M. Hoversten, K. Key, and J. Chen, 2012, Resolution of reservoir scale electrical anisotropy from marine CSEM data: *Geophysics*, **77**, no. 2, E147–E158, doi: [10.1190/geo2011-0159.1](https://doi.org/10.1190/geo2011-0159.1).
- Chave, A. D., and C. S. Cox, 1982, Controlled electromagnetic sources for measuring electrical-conductivity beneath the oceans. Part 1: Forward problem and model study: *Journal of Geophysical Research*, **87**, 5327–5338, doi: [10.1029/JB087iB07p05327](https://doi.org/10.1029/JB087iB07p05327).
- Constable, S., 2010, Ten years of marine CSEM for hydrocarbon exploration: *Geophysics*, **75**, no. 5, 75A67–75A81, doi: [10.1190/1.3483451](https://doi.org/10.1190/1.3483451).
- Constable, S., R. L. Parker, and C. G. Constable, 1987, Occam's inversion — A practical algorithm for generating smooth models from electromagnetic sounding data: *Geophysics*, **52**, 289–300, doi: [10.1190/1.1442303](https://doi.org/10.1190/1.1442303).
- Constable, S., and C. J. Weiss, 2006, Mapping thin resistors and hydrocarbons with marine EM methods: Insights from 1D modeling: *Geophysics*, **71**, no. 2, G43–G51, doi: [10.1190/1.2187748](https://doi.org/10.1190/1.2187748).
- Key, K., 2009, 1D inversion of multicomponent, multifrequency marine CSEM data: Methodology and synthetic studies for resolving thin resistive layers: *Geophysics*, **74**, no. 2, F9–F20, doi: [10.1190/1.3058434](https://doi.org/10.1190/1.3058434).
- Key, K., 2012, Marine EM inversion using unstructured grids: A 2D parallel adaptive finite element algorithm: 82nd Annual International Meeting, SEG, Expanded Abstracts, doi: [10.1190/segam2012-1294.1](https://doi.org/10.1190/segam2012-1294.1).
- Key, K., and J. Owall, 2011, A parallel goal-oriented adaptive finite element method for 2.5-D electromagnetic modelling: *Geophysical Journal International*, **186**, 137–154, doi: [10.1111/j.1365-246X.2011.05025.x](https://doi.org/10.1111/j.1365-246X.2011.05025.x).
- Loseth, L. O., H. M. Pedersen, B. Ursin, L. Amundsen, and S. Ellingsrud, 2006, Low-frequency electromagnetic fields in applied geophysics: Waves or diffusion?: *Geophysics*, **71**, no. 4, W29–W40, doi: [10.1190/1.2208275](https://doi.org/10.1190/1.2208275).
- Myer, D., S. Constable, and K. Key, 2013, Magnetotelluric evidence for layered mafic intrusions beneath the Vøring and Exmouth rifted margins: *Physics of The Earth and Planetary Interiors*, **220**, 1–10, doi: [10.1016/j.pepi.2013.04.007](https://doi.org/10.1016/j.pepi.2013.04.007).
- Myer, D., S. Constable, K. Key, M. E. Glinsky, and G. Liu, 2012, Marine CSEM of the Scarborough gas field. Part 1: Experimental design and data uncertainty: *Geophysics*, **77**, no. 4, E281–E299, doi: [10.1190/geo2011-0380.1](https://doi.org/10.1190/geo2011-0380.1).
- Ramananjaona, C., L. MacGregor, and D. Andréis, 2011, Sensitivity and inversion of marine electromagnetic data in a vertically anisotropic stratified earth: *Geophysical Prospecting*, **59**, 341–360, doi: [10.1111/j.1365-2478.2010.00919.x](https://doi.org/10.1111/j.1365-2478.2010.00919.x).
- Ray, A., and K. Key, 2012, Bayesian inversion of marine CSEM data with a trans-dimensional self parametrizing algorithm: *Geophysical Journal International*, **191**, 1135–1151, doi: [10.1111/j.1365-246X.2012.05677.x](https://doi.org/10.1111/j.1365-246X.2012.05677.x).
- Ward, S. H., and G. W. Hohmann, 1987, Electromagnetic theory for geophysical applications, in M. N. Nabighian, ed., *Electromagnetic methods in applied geophysics*: SEG, 131–311.
- Weidelt, P., 2007, Guided waves in marine CSEM: *Geophysical Journal International*, **171**, 153–176, doi: [10.1111/j.1365-246X.2007.03527.x](https://doi.org/10.1111/j.1365-246X.2007.03527.x).